Biophysical Journal, Volume *111*

Supplemental Information

Glycolipid Crosslinking Is Required for Cholera Toxin to Partition Into and Stabilize Ordered Domains

Krishnan Raghunathan, Tiffany H. Wong, Daniel J. Chinnapen, Wayne I. Lencer, Michael G. Jobling, and Anne K. Kenworthy

Supporting material

Glycolipid crosslinking is required for cholera toxin to partition into and stabilize ordered domains

Krishnan Raghunathan,[*] Tiffany H. Wong,[*] Daniel J. Chinnapen,[†] Wayne I. Lencer, [†] Michael G. Jobling,[¶] Anne K Kenworthy, [*,§]

[*]Department of Molecular Physiology and Biophysics, Vanderbilt University School of Medicine, Nashville, Tennessee, USA [†]Harvard Medical School and the Harvard Digestive Diseases Center, Boston, Massachusetts, USA; [¶]Department of Immunology and Microbiology, University of Colorado Anschutz Medical Campus, Aurora, Colorado, USA; [§]Department of Cell and Developmental Biology, Vanderbilt University School of Medicine, Nashville, Tennessee, USA

Supplementary Text

Supplementary Text S1: Defining some commonly used terminology

Raft Marker vs. Raft Inducer vs. Raft stabilizer: If a molecule preferentially partitions into the ordered phase, it is termed as a "raft marker" (1). We define a raft partition coefficient as

$$P_{raft} = \frac{C_{raft}}{C_{raft} + C_{non-raft}}$$

where C is the concentration in a particular phase, usually measured using fluorescence microscopy (1). WT-CTxB is enriched in the ordered phase and hence WT-CTxB is a raft marker. Using the above definition, a raft marker would have a raft partition coefficient greater than 0.5. If a molecule increases the propensity for ordered phase to form, it is called as a "raft inducer." As an example, in our experiments, we find that WT-CTxB increases T_{misc}. This means addition of CTxB facilitates liquid-liquid phase separation and thus induces raft formation. Any process that favors the formation of the ordered phase is also considered to "stabilize" raft domains. "Raft inducer" and "raft stabilizer" are often used to describe similar phenomena (2, 3) and potentially could imply identical characteristics (4, 5). In this manuscript, we have used the two terms interchangeably. Although CTxB is both a raft marker and raft inducer/raft stabilizer, these two behaviors are not necessarily coupled: a molecule can preferentially partition into the disordered phase and still function as a raft inducer (6, 7).

Raft marker vs. Lipid raft affinity: A term related to "raft marker" is the concept of "lipid raft affinity." Preferential lipid raft partitioning of CTxB could arise either as a consequence of its ability to cluster multiple GM1 or because it binds to only a subset of GM1 that are oriented in a distinct manner in the ordered phase. While in both cases, WT-CTxB behaves as a raft marker, only in the latter case can we say that the CTxB has a lipid raft affinity. Because our experiments cannot distinguish between these two possibilities, we avoid the use of the term lipid raft affinity in this manuscript.

Nanoclustering versus Nanodomains: "Nanodomains" refers to organization of membranes that have properties similar to the liquid ordered/disordered phases seen in the micron sized phase separation but are only nanometer scale in size. "Nanoclusters" on the other hand, need not imply phase separation but refer to a physical organization of molecules. In our case, binding of WT CTxB to five GM1 molecules could result in the formation of a nanocluster in the membrane, but need not necessarily induce nanodomain formation.

Interestingly, in recent work, it has been shown that there exist two types of nanodomains when CTxB binds to GM1 in GUVs, depending on the concentration of CTxB and the lipid composition of the GUVs

(8). One is a traditional nanodomain which is formed even without the addition of CTxB but which the authors speculate can be further clustered by crosslinking into micron sized domains that are observed in microscopy experiments. The second is a novel form of nanodomain which is more transient and is generated only as a consequence of crosslinking by CTxB. These results have been strengthened further through simulations showing that nanoscale crosslinking by CTxB modulates local nanoscale order through lipid interactions (9).

Supplementary Text S2: Understanding the relationship between nanoclustering and micron-sized domain formation

In subsequent paragraphs, we will discuss the possible relationship between micron-scale domain formation and nano-scale membrane organization in context of our results viz. CTxB increasing T_{misc} in a concentration-dependent manner.

It is known that composition of isolated plasma membrane is close to a miscibility critical point (10). Thus, the miscibility transition temperature T_{misc} is the critical temperature of the mixture. This implies that even above the miscibility temperature, fluctuations in the membrane persist (10). Ising model calculations have been used to calculate the size of fluctuations (10). These models predict that the micron-sized fluctuations that exist as co-existing liquid phases in GPMVs would be tens of nanometers at physiological temperature (10, 11). These fluctuations are thought to be the basis of lipid rafts in cells (10). For our results, this would have straightforward implications: increasing the transition temperature of GPMVs by clustering GM1 would increase the size and stability of nanoscale domains at physiological temperature (12). Thus, from a simplistic standpoint, this would imply nanoscale clustering by CTxB could "stabilize" nanoscale domains by increasing local membrane order (6). This relationship is also expanded further in Supplementary Text S3. However, as appealing as this theory might be, in the narrow context of our results with CTxB, there are a few fundamental limitations of this model.

First, we typically use 1 μg/ml of toxins in our studies and this produces the observed ~5 ºC change in transition temperature. In cell based studies, it is known that at least, two orders of magnitude lower concentrations of toxin can induce cellular intoxification (13). The corresponding change in transition temperature for such a low toxin concentration would be negligible (~0.05 ºC) based on our results, assuming that the change in T_{misc} remains linear as a function of toxin concentration. Thus, based on criticality model, such low concentrations of CTxB would not be predicted to stabilize micron-sized domains. However, to carry out its biological functions, nano-scale clustering of CTxB and/or CTxB-enriched nanodomains are more physiologically relevant than micron-scale domains. We would also like to note that use of Ising Models in understanding emergent behavior of membranes is still in its infancy. It is, for instance, possible to expand the model to accommodate more parameters such as nanoscale clustering or local curvature introduced by CTxB in the plasma membrane akin to actin pinning (14) which would then help us understand how low concentrations of CTxB influence membrane remodeling. However, in our view, at present, the relationship between nanoclusters, nanodomains, and micron-sized domains is still unclear.

Second and more importantly, not all lipid mixtures are critical. While critical behavior is reported for plasma membrane isolated from some cell lines, it is not known if this behavior is universal or occurs in a cellular context. However, it is important to understand that the relationship between lipid phases and "nanoscale" rafts predates the discovery of critical behavior in plasma membranes (15, 16). Indeed, most studies involving GUVs do not use critical compositions of lipids. The original (and potentially still most relevant) premise behind the use of GUVs in understanding lipid rafts is that the compositional variation leads to domain formation, stability, size and morphology (17). Thus, while criticality theory implies nano-scale domains could be related to micron scale phases, this might not be the case.

Another potential complication is the role of membrane curvature. It is known that phase separation, lipid sorting and membrane curvature are intricately coupled (18). This relationship potentially forms the bedrock for any physical basis for understanding the relationship between lipid rafts and endocytosis of cargoes such as cholera toxin. It has been hypothesized for Shiga toxin which clusters the glycolipid Gb3, that lipid clustering could lead to membrane curvature changes (19). Similarly, clustering of GM1 by the virus SV40 and CTxB has been shown to induce membrane tubulation (20). However, the relationship

between phase separation, sorting and membrane curvature is not entirely clear and more work needs to be done in this regard.

Supplementary Text S3: Potential relationship between raft preference and domain stabilization

From a physical standpoint, our two results, stabilization of domains and phase preference of pentavalent WT CTxB, represent two distinct aspects of lipid rafts. It is tantalizing to think of these two behaviors as manifestations of criticality critical behavior of phases in isolated the plasma membrane (10). According to the criticality model of membrane organization, the plasma membrane is compositionally proximal to a binary liquid mixture and the compositional fluctuations arising as a consequence of criticality correspond to lipid rafts in cells (10). For a critical binary liquid, it is known that an increase in its miscibility transition temperature can result when a molecule preferentially sorts into one phase (11). This implies that the penchant preference for pentavalent CTx to associate with GM1 in ordered phase can drive the increased heterogeneity by stabilizing the ordered phase, explaining both sets of results.

Supplementary Methods

Materials

DiI-C12, Fast-DiO and Alexa Fluor 647 goat anti mouse IgG (H+L) were purchased from Life Technology (Eugene, USA). COS-7 and RBL-2H3 cell lines were acquired from ATCC (Manassas, USA). DTT was purchased from Research Products International (Mount Prospect, USA) and was made fresh for every single use. Para-formaldehyde was purchased as solid from Fisher Scientific and prepared as a 37% stock solution in water. All other chemicals ($CaCl_2$, Hepes and NaCl) were purchased from Sigma. Anti-beta subunit CTx antibody (ab62429) was purchased from Abcam.

Cell Culture

COS-7 cells were maintained in Dulbecco's modified Eagle medium (DMEM) containing 10% fetal bovine serum (FBS), 1% Pen/Strep at 37 ºC and 5% CO_2. RBL-2H3 cells were grown in MEM media with 10% FBS, 1% Pen/Strep at 37º C and 5% CO_2. For all studies, cells were freshly plated a day prior to the experiments such that they would be 70-80% confluent on the day of the experiment.

Preparation of monovalent CTx and CTxB

Alexa 568 monovalent CTx and wild type CTx were prepared as described previously (13, 21). Although a reduction in the number of functional GM1 binding sites decreases the avidity of binding of monovalent CTx to GM1 tenfold compared to WT CTx (13), the binding site substitutions do not affect the ability of the B-subunit to assemble into homopentamers. Thus, the B pentamers are otherwise structurally similar in WT and monovalent variants of CTx.

For unknown reasons, the holotoxin system (13) could not be adapted for production of CTxB pentamers alone. We therefore developed a novel expression system that consistently produced pentamers with defined ratios of subunits. A population of CTxB pentamers with variable numbers of binding sites was produced by IPTG induction of *E. coli* TE1 (22) carrying an expression vector consisting of a *lacUV5* promoter, a *ctxB* gene encoding the G33D substitution (inactivating GM1 binding,(23, 24)), the native transcriptional terminator from the *ctx* operon, followed by a wt *ctxB* gene with a 3′ extension encoding a glycosylation-sulfation-his_6 tag (25). The glycosylation-sulfation tag has been used to monitor intracellular trafficking of heat-labile enterotoxins (26), and addition of his_6 to this tag decreased protease susceptibility during purification (not shown, (13)). While addition of the tag reduced toxicity of holotoxins with 5 wt binding sites (BS) and one or two tagged B subunits, the tags did not appear to directly affect GM1 binding (13) consistent with the C-terminus of the native B subunit being situated on the upper surface of the pentamer and well removed from the GM1 BS (24, 27). Its purpose in this study is solely to permit separation and purification of the variant CTxB pentamers with a single GM1 BS. The native terminator attenuates expression of the second *ctxB* gene from the proximal *lacUV5* promoter such that the pentamers produced consist of native-sized G33D and C-terminally tagged wt monomers more or less randomly assembled in an approximately 4:1 ratio (G33D to wt binding sites). A second preparation was produced from TE1 carrying an alternate clone encoding wt CTxB followed by G33D-tagged subunits, which reversed the ratio of binding sites in the mixed penatamers.

From both preparations, mixed pentamers were purified from induced cell extracts by Talon (metal-ion affinity) chromatography and further separated into individual species by ion-exchange chromatography with a salt gradient elution (0-16% 1M NaCl over 40 column volumes) on a GE-AKTA essentially as described by Jobling et al. with minor modifications (13). Untagged B pentamers (B5 0 BS [or 5BS]) did not bind and eluted in the column flow through (figure S3, showing G33D+wt-tagged preparation; [wt+G33D-tagged preparation], not shown), single tagged pentamers (B4-T1, 1 BS [or 4BS]) eluted as a major peak (mAU_{280nm}) showing minor interaction with the column and a secondary peak (B4-T1#) eluting with the salt gradient; B3-T2 and B3-T2# (2 [or 3] BS) eluted in the next two peaks with increased salt gradient. Peak fractions were pooled, desalted and concentrated by buffer-exchange into PBS, and examined by SDS-PAGE (Supplementary Figure 1 inset). Upper gel is unboiled samples by 10% SDS-PAGE with composition and number of binding sites shown above each lane. Under these conditions CTxB migrates as assembled pentamers – wt CTxB5 migrating with M_r of 50 kDa, CTxB5 (G33D) with an M_r of 130 kDa likely due to a combination of factors that includes altered charge or reduced SDS-binding. Each pooled fraction migrates as an essentially pure species with defined mobility. Lower gel is 15% SDS-PAGE with boiled and reduced samples that separate into individual monomers, native CTxB with

an M_r of 11 kDa (expected 11.6 kDa) and tagged monomers with an M_r of 15 kDa (expected 15.1 kDa), showing the expected ratios of either 0, 1 or 2 tagged monomers with 5, 4 or 3 native-sized monomers.

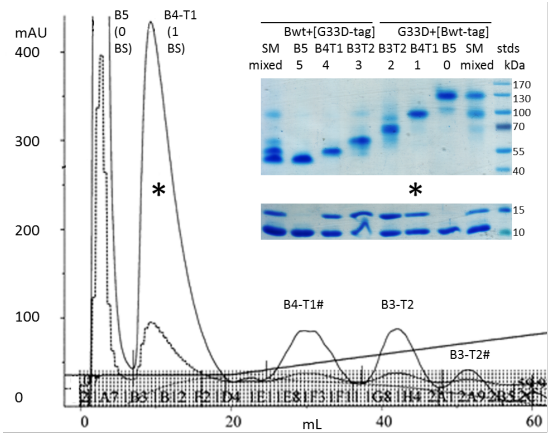

Supplementary Figure 1: Purification of single binding site CTxB. Mixed pentamers from two preparations (Bwt+G33D-tag and G33D+Bwt-tag) were fractionated by ion-exchange chromatography with a salt gradient elution (shallow sloping solid line; 60 ml elution approximates to 20 column volumes or 8% gradient). Peaks are labeled with subunit composition as described in the methods. Fractions were pooled, concentrated and analyzed by SDS-PAGE (inset). Annotations above each lane show, in order, expression clone used, subunit composition (B, native sized or T, tagged subunit; SM starting material), and number of expected binding sites per pentamer (mixed for SM preparations). SM in the gel denotes the starting material. Asterisks mark the single binding site species (column peak, pentamer [upper gel] and monomer composition [lower gel]) used in this study. Peak denoted as # in the figure represents a secondary peak which when analyzed by SDS-PAGE had the same mobility/monomer ratios, but differed in their ability to interact with the ion-exchange resin.

Proteins were detected by colloidal staining with Coomassie Blue G250 (28).

Monovalent CTxB and wild type CTxB were labeled using the tetrafluorophenyl (TFP) ester of Alexa Fluor 488 (ThermoFisher, MA) and reaction products separated with the provided size-exclusion matrix from the kit. Briefly, 0.5 mg of monovalent or wild type CTxB were exchanged into bicarbonate buffer pH 8.3 and added to the TFP ester at a concentration of 1 mg/mL. The mixture was allowed to react with stirring for one hour at room temperature. Labeling reactions were added to Bio-Rad P30 BioGel for column separation. The early eluting “labeled” protein was collected and measured for degree of labeling. Using the above protocol**,** each CTxB pentamer was labeled with approximately 1.8 Alexa fluorophores.

Preparation of Giant Plasma Membrane Vesicles

GPMVs were prepared as previously described (12). Cells were washed with Phosphate Buffer Saline (PBS) twice. They were then incubated with the appropriate dye (DiI-C12, 0.5 µg/ml final concentration or Fast-DiO, 5 µg/ml final concentration) in PBS at 37º C for 10 minutes. The cells were subsequently washed with GPMV buffer (2 mM $CaCl_2$ /10 mM Hepes /0.15M NaCl, pH 7.4), twice. Cells were then finally incubated in GPMV active buffer (GPMV buffer described above along with 25 mM formaldehyde and 2 mM DTT) for up to two hours at 37º C with shaking at 100 RPM. The GPMV-containing supernatant was then decanted into a centrifuge tube.

For most experiments, GPMVs were treated with CTxB or CTx after isolation. To do so, the appropriate concentration of CTxB or CTx was added to 100-250 µl of the decanted GPMV solution and used for imaging. The remainder of the decanted solution was used as the untreated control for the experiments. In the second set of control experiment, cells were pre-treated with CTxB prior to GPMV isolation. For the pre-treatment experiments, the cells were first co-incubated with both DiI-C12 and 1µg/ml CTxB-Alexa

488 for 10 min at 37 ºC and GPMVs were then isolated as described above. Transition temperatures were measured in these experiments relative to GPMVs isolated from a sister plate of cells (plated identically) prepared the same way as the treated but without the CTxB.

For the antibody labeling experiments, GPMVs were isolated and labeled with CTxB or mCTxB as indicated above. A portion of the toxin labeled samples were then subjected to further labeling with either anti-CTB antibody (1:200) or anti-CTB (1:200) followed by Alexa Fluor 647 goat anti mouse IgG (H+L) antibody (1:200). Each antibody labeling step was performed for at least one hour at room temperature before imaging.

Confocal Imaging

GPMVs were imaged using a Zeiss LSM 510 confocal microscope using a 40X 1.2 NA Zeiss Plan-Neofluor objective. The confocal pinhole was set at 5 airy units for all experiments. The fluorophores were excited using the 488 nm line of a 40 mW Argon laser (Alexa-488 or Fast DiO), 543 nm line of a HeNe laser (Alexa 568 or DiI-C12), or 633 nm line of a HeNe laser (Alexa 647). Images were collected at 1X digital zoom for transition temperature measurements and 8-10X digital zoom for quantifying raft localization. The stage was cooled using a Linkam Peltier Cooling system (Tadworth, UK).

Measurement of Transition Temperature (T_{misc}) Change

Images of GPMVs were manually classified as being phase separated or containing a single uniform phase. The fraction of vesicles that were phase separated at each temperature was then calculated. This curve was fit to a sigmoidal function and the transition temperature (T_{misc}) was defined as the temperature at which 50% of GPMVs are phase separated (29). Since the magnitude of T_{misc} can be dependent on cell type and other growth conditions, T_{misc} was reported with respect to an untreated control (12). At least three independent experiments were performed on different days for each CTxB concentration for T_{misc} measurements. For each temperature of each repeat, at least 20 GPMVs were imaged and classified.

Quantifying Raft partitioning

For all the raft partitioning experiments, cells were pre-labeled with a disorder phase marker (either DiI-C12 or Fast-DiO) prior to GPMV isolation as described above. The isolated GPMVs were subsequently labeled with 1µg/ml wild type or monovalent Alexa 568-CTx or Alexa 488-CTxB. DiI-C12 was used in

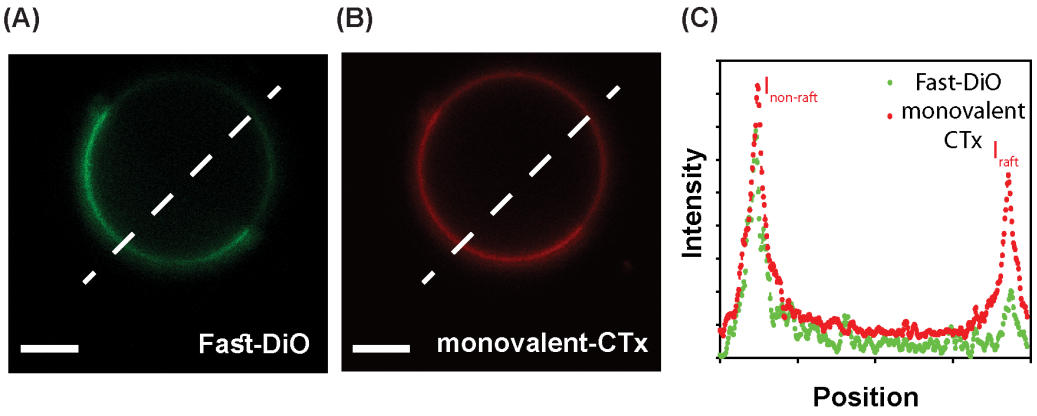

Supplementary Figure 2: Quantification of raft partitioning. (A,B) A representative GPMV labeled with Fast-DiO (A) as the disordered phase marker and monovalent-CTx (B). The white dashed line represents a typical line scan. (C) The line scan of the fluorescence intensities of the two channels is shown. The peaks correspond to the fluorescence intensity of the disordered phase markers and mCTx in the GPMV.

combination with Alexa 488-labeled CTxB and mCTxB, and Fast DiO was used in combination with Alexa 568-labeled CTx and monovalent CTx. To determine the phase partitioning of wild type and monovalent

CTx and CTxB, we imaged single GPMVs in the green and red channels sequentially. Experiments for CTx and CTxB were performed independently.

Typically, experiments were performed using a cooling stage held at 5-10 ºC. To analyze the data, a line scan across a single GPMV was performed in both the channels using ImageJ software to determine the fluorescence intensity at every pixel. The position of the line was set so that it intersected both an ordered and disordered region of the GPMV using the disordered phase channel as the reference (Supplementary Figure 2A). The same line was used to analyze the cholera toxin channel (Supplementary Figure 2B). The line scans were smoothened using a moving average (5 pixels) in Microsoft Excel. A raft partitioning coefficient P_{raft} was then calculated as previously described (1) as

$$P_{raft} = \frac{I_{raft}}{I_{raft} + I_{non-raft}}$$

where I_{raft} and $I_{non\text{-}raft}$ are the fluorescence intensity of the CTxB channel in the ordered and disordered phases, respectively, as defined by the peaks in the line scan (Supplementary Figure 2C). A summary of the results of the raft partitioning measurements reported in each figure is provided in Supplementary Table 1.

Supplementary Table 1. Summary of raft partitioning measurements.

Figure	Toxin	# GPMVs	# Independent Experiments	Raft Partition Coeff Mean ± Std Dev
Figure 2	WT CTx (holotoxin)	12	2	0.57 ± 0.06
	WT CTxB	31	3	0.57 ± 0.05
	Monovalent CTx (holotoxin)	66	4	0.49 ± 0.10
	Monovalent CTxB	24	3	0.44 ± 0.06
Supplementary Figure 3	Monovalent CTxB	49	2	0.55 ± 0.12
	WT CTxB	58	2	0.64 ± 0.11
	Monovalent CTxB + Anti CTxB (mouse)+ Alexa 647 Anti-mouse (secondary)	56	2	0.84 ± 0.08
	WT CTxB + Anti CTxB (mouse)+ Alexa 647 Anti-mouse (secondary)	37	2	0.72 ± 0.10
Supplementary Figure 4	WT CTxB 0.2µg/ml	38	2	0.62 ± 0.08

Statistical analysis

Data for the changes to transition temperature are represented as the mean ± the standard error of the mean (SEM). Student t-test was used to compare all pairs of data. $P<0.05$ was deemed as significant.

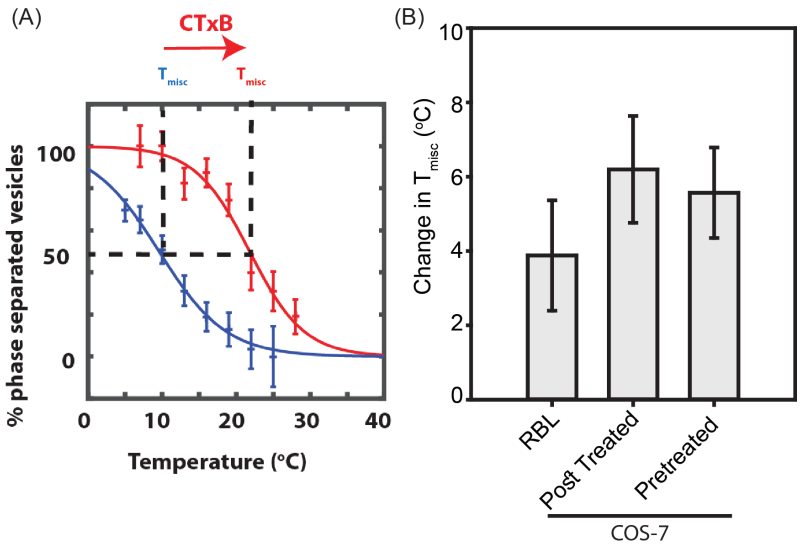

Supplementary Figure 3: Method used to calculate T_{misc} and associated control experiments. (A) T_{misc} is increased in RBL-derived GPMVs incubated with 1μg/ml CTxB (red) compared to untreated control GPMVs (blue). Error bars show SEM. (B) Average increase in T_{misc} upon treatment with 1μg/ml CTxB for GPMVs isolated from RBL cells or COS-7 cells relative to untreated control GPMVs. Also shown is the average increase in T_{misc} for GPMVs isolated from COS-7 cells pretreated with 1μg/ml CTxB for 10 min at 37 ºC relative to GPMVs isolated from untreated control cells.

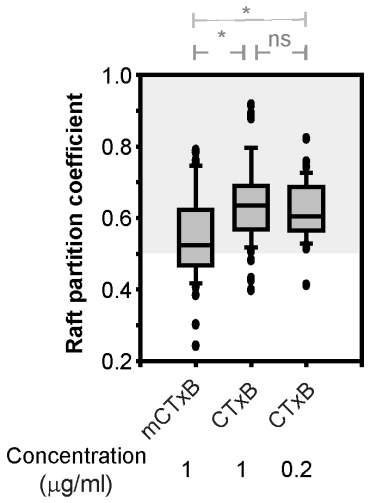

Supplementary Figure 4: Effect of low concentrations of CTxB on raft partition coefficients. Comparison of raft partitioning coefficient of COS-7 cells GPMVs labeled with 1 μg/ml monovalent CTxB (mCTxB), 1 μg/ml WT CTxB, or 0.2 μg/ml WT CTxB. Statistically, we find no significant difference in raft partitioning between the two concentrations of WT CTxB. However, both were significantly higher than the raft partitioning coefficient of monovalent CTxB (ns, not significant; *, $p < 0.05$). Thus, the difference in partitioning between the monovalent and wild type toxin was not a consequence of the decreased avidity of binding of monovalent compared to the WT toxins.

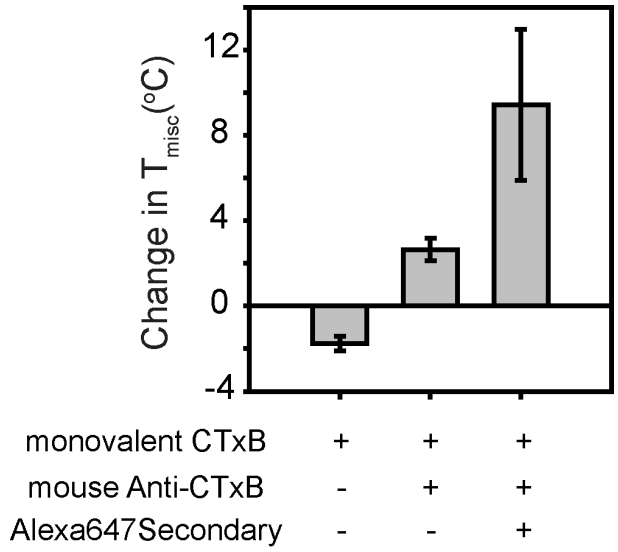

Supplementary Figure 5: Effect of antibody crosslinking on T_{misc}. Change in T_{misc} for GPMVs isolated from COS-7 cells incubated with 1µg/ml monovalent CTxB-488 alone, monovalent CTxB-488 and mouse anti-CTxB (1:200 dilution), or monovalent CTxB-488, mouse anti-CTxB (1:200), and Alexa Fluor 647 goat anti mouse IgG (H+L) (1:200).

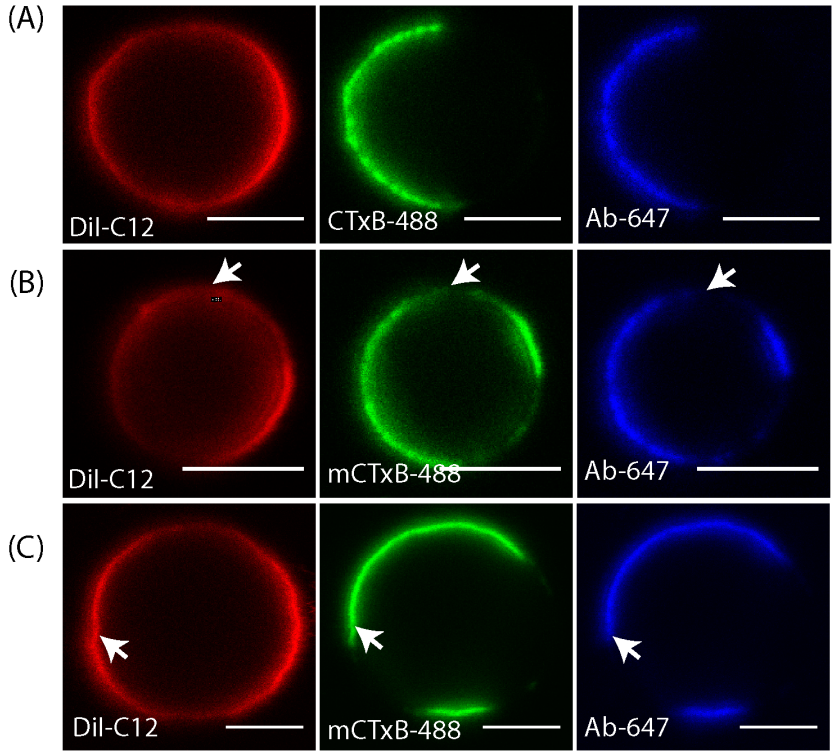

Supplementary Figure 6: Representative images showing the effect of antibody crosslinking on raft partitioning. Representative images of COS-7 GPMVs labeled with WT CTxB **(A)** or monovalent CTxB **(B, C)** and subsequently crosslinked with mouse anti-CTB (1:200) and Alexa Fluor 647 goat anti mouse IgG (H+L) (1:200). Note that in these experiments, the crosslinked CTxB domains occasionally partially overlapped with both the ordered and disordered domains in the same GPMV. For example, in (B), a portion of the ordered domain does not contain crosslinked toxin again as indicated by the arrow. In (C), mCTB forms a distinct domain primarily in the liquid ordered domain, but the boundary of the domain extends into the disordered phase as well as indicated by the arrow. These behaviors were seen for both monovalent and WT toxin following antibody crosslinking. In such cases, for the calculation of the raft partition coefficient, the DiI-C12 channel was as a reference to draw the line scan while ensuring the toxin channel was accurately represented. For instance, in (B), the line would pass through the ordered phase where the toxin channel is distinctly visible and in (C) it would pass through the disordered where there is practically no toxin. We should note that this could result in overestimation of the raft partition coefficient. However, as seen in the representative images, this effect of clustering by antibody was extremely distinct from pentavalent binding of CTxB. Scale bars, 5 μm.

.

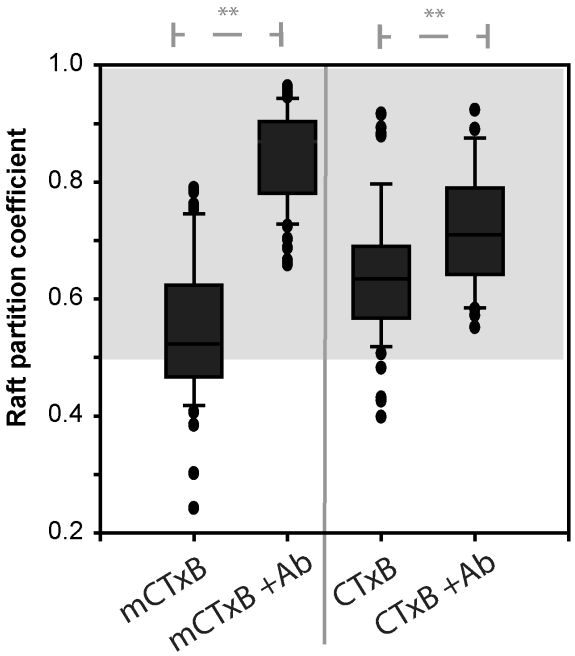

Supplementary Figure 7: Antibody crosslinking enhances raft partitioning of both monovalent CTxB and WT CTxB. Raft partitioning coefficients were calculated for COS-7 GPMVs labeled with either monovalent CTxB or WT CTxB alone or with monovalent CTxB or WT CTxB followed by mouse anti-CTB (1:200) and Alexa Fluor 647 goat anti mouse IgG (H+L) (1:200) (designated as “+ Ab" in the figure.) Note that relative to Figure 2, the partition coefficients of both mCTxB and wt CTxB are slightly higher, likely because they were performed with a different passage of cells. **, $p < 0.01$.

Supporting references

1. Sezgin, E. et al. 2012. Partitioning, diffusion, and ligand binding of raft lipid analogs in model and cellular plasma membranes. Biochim. Biophys. Acta - Biomembr. 1818: 1777–1784.
2. Lingwood, D. et al. 2008. Plasma membranes are poised for activation of raft phase coalescence at physiological temperature. Proc. Natl. Acad. Sci. U. S. A. 105: 10005–10010.
3. Bacia, K. et al. 2005. Sterol structure determines the separation of phases and the curvature of the liquid-ordered phase in model membranes. Proc. Natl. Acad. Sci. U. S. A. 102: 3272–7.
4. London, E. 2005. How principles of domain formation in model membranes may explain ambiguities concerning lipid raft formation in cells. Biochim. Biophys. Acta - Mol. Cell Res. 1746: 203–220.
5. Wenz, J.J. and F.J. Barrantes. 2003. Steroid structural requirements for stabilizing or disrupting lipid domains. Biochemistry. 42: 14267–14276.
6. Levental, K.R. et al. 2016. Polyunsaturated lipids regulate membrane domain stability by tuning membrane order. Biophys. J. 110: 1800–1810.
7. Putzel, G.G. and M. Schick. 2009. Theory of raft formation by the cross-linking of saturated or unsaturated lipids in model lipid bilayers. Biophys. J. 96: 4935–4940.
8. Štefl, M. et al. 2012. Dynamics and size of cross-linking-induced lipid nanodomains in model membranes. Biophys. J. 102: 2104–2113.
9. Sun, H. et al. 2015. Nanodomain formation of ganglioside GM1 in lipid membrane: Effects of Cholera toxin mediated crosslinking. Langmuir. 31: 9105–14.
10. Veatch, S.L. et al. 2008. Critical fluctuations in plasma membrane vesicles. ACS Chem. Biol. 3: 287–93.
11. Machta, B.B. et al. 2012. Critical casimir forces in cellular membranes. Phys. Rev. Lett. 109: 1–5.
12. Raghunathan, K. et al. 2015. Membrane transition temperature determines cisplatin response. PLoS One. 10: e0140925.
13. Jobling, M.G. et al. 2012. A single native ganglioside GM1-binding site is sufficient for cholera toxin to bind to cells and complete the intoxication pathway. MBio. 3: 1–9.
14. Honigmann, A. et al. 2014. A lipid bound actin meshwork organizes liquid phase separation in model membranes. Elife. 3: e01671.
15. Edidin, M. 2003. The state of lipid rafts: from model membranes to cells. Annu. Rev. Biophys. Biomol. Struct. 32: 257–283.
16. Simons, K. and W.L.C. Vaz. 2004. Model systems, lipid rafts, and cell membranes. Annu. Rev. Biophys. Biomol. Struct. 33: 269–295.
17. De Almeida, R.F.M. et al. 2005. Lipid rafts have different sizes depending on membrane composition: A time-resolved fluorescence resonance energy transfer study. J. Mol. Biol. 346: 1109–1120.
18. Tian, A. and T. Baumgart. 2009. Sorting of lipids and proteins in membrane curvature gradients. Biophys. J. 96: 2676–2688.
19. Safouane, M. et al. 2010. Lipid cosorting mediated by Shiga toxin induced tubulation. Traffic. 11: 1519–1529.
20. Ewers, H. et al. 2010. GM1 structure determines SV40-induced membrane invagination and infection. Nat. Cell Biol. 12: 11-18–12.
21. Day, C.A. et al. 2015. Microtubule motors power plasma membrane tubulation in clathrin-independent endocytosis. Traffic. 16: 572–590.
22. Jobling, M.G. and R.K. Holmes. 2000. Identification of motifs in cholera toxin A1 polypeptide that are required for its interaction with human ADP-ribosylation factor 6 in a bacterial two-hybrid

system. Proc. Natl. Acad. Sci. U. S. A. 97: 14662–7.

23. Jobling, M.G. and R.K. Holmes. 1991. Analysis of structure and function of the B subunit of cholera toxin by the use of site-directed mutagenesis. Mol. Microbiol. 5: 1755–1767.

24. Merritt, E.A. et al. 1997. Structural studies of receptor binding by cholera toxin mutants. Protein Sci. 6: 1516–1528.

25. Wolf, A.A. et al. 2008. Attenuated endocytosis and toxicity of a mutant cholera toxin with decreased ability to cluster ganglioside GM1 molecules. Infect. Immun. 76: 1476–1484.

26. Fujinaga, Y. et al. 2003. Gangliosides that associate with lipid rafts mediate transport of cholera and related toxins from the plasma membrane to endoplasmic reticulm. Mol. Biol. Cell. 14: 4783–4793.

27. Liljeqvist, S. et al. 1997. Fusions to the cholera toxin B subunit: Influence on pentamerization and GM1 binding. J. Immunol. Methods. 210: 125–135.

28. Kang, D. et al. 2002. Highly sensitive and fast protein detection with coomassie brilliant blue in sodium dodecyl sulfate-polyacrylamide gel electrophoresis. Bull. Korean Chem. Soc. 23: 1511–1512.

29. Gray, E. et al. 2013. Liquid general anesthetics lower critical temperatures in plasma membrane vesicles. Biophys. J. 105: 2751–9.